Review of Scientific Instruments

100 MHz large bandwidth preamplifier and record-breaking 50 kHz scanning rate quantum point contact mode probe microscopy imaging with atomic resolution

Cite as: Rev. Sci. Instrum. **92**, 013701 (2021); https://doi.org/10.1063/5.0024802
Submitted: 13 August 2020 . Accepted: 11 December 2020 . Published Online: 07 January 2021

Quan Feng Li, Yang Wang, Fang Wang, Yubin Hou, and Qingyou Lu

Review of Scientific Instruments | ARTICLE | scitation.org/journal/rsi

100 MHz large bandwidth preamplifier and record-breaking 50 kHz scanning rate quantum point contact mode probe microscopy imaging with atomic resolution

Cite as: Rev. Sci. Instrum. 92, 013701 (2021); doi: 10.1063/5.0024802
Submitted: 13 August 2020 • Accepted: 11 December 2020 •
Published Online: 7 January 2021

View Online Export Citation CrossMark

Quan Feng Li,[1,a)] Yang Wang,[1] Fang Wang,[2] Yubin Hou,[3] and Qingyou Lu[3,4,a)]

AFFILIATIONS

[1] Henan Key Laboratory of Photovoltaic Materials, School of Physics, Henan Normal University, Xinxiang 453007, People's Republic of China
[2] College of Electronic and Electrical Engineering, Henan Normal University, Xinxiang 453007, Henan, People's Republic of China
[3] Anhui Province Key Laboratory of Condensed Matter Physics at Extreme Conditions, High Magnetic Field Laboratory, Chinese Academy of Sciences, Hefei 230031, Anhui, People's Republic of China
[4] Hefei National Laboratory for Physical Sciences at the Microscale, University of Science and Technology of China, Hefei, Anhui 230026, People's Republic of China

[a)] **Authors to whom correspondence should be addressed:** lqfeng@mail.ustc.edu.cn and qxl@ustc.edu.cn

ABSTRACT

The high-bandwidth preamplifier is a vital component designed to increase the scanning speed of a high-speed scanning tunneling microscope (STM). However, the bandwidth is limited not only by the characteristic GΩ feedback resistor R_F but also by the characteristic unity-gain-stable operational amplifier (UGS-OPA) in the STM preamplifier. Here, we report that paralleling a resistor with the tunneling junction (PRTJ) can break both limitations. Then, the UGS-OPA can be replaced by a higher rate, higher antinoise ability, decompensated OPA. By doing so, a bandwidth of more than 100 MHz was achieved in the STM preamplifier with decompensated OPA657, and a higher bandwidth is possible. High-clarity atomic resolution STM images were obtained under about 10 MHz bandwidth and quantum point contact microscopy mode with a record-breaking line rate of 50 k lines/s and a record-breaking frame rate of 250 frames/s. Both the PRTJ method and the decompensated OPA will pave the way for higher scanning speeds and play a key role in the design of high-performance STMs.

I. INTRODUCTION

The scanning tunneling microscope (STM) with high-speed (HS) scanning capability is a crucial tool in surface science and technology.[1–5] It has revealed the mechanism of dynamic phenomena at the atomic scale: the growth mechanism of graphene,[4] for example. Inevitably, it will also be a tool for high-speed readout in atomic-scale data storage devices.[3] The femtosecond (fs) laser STM[6] and electronic pump-probe radio STM can only investigate dynamic processes with a spectrum, but their imaging speeds are also conventional.[7] Accordingly, many groups are devoting themselves to the development of high-speed imaging STMs.[8–12] However, progress in this direction is greatly restricted by not only the limited bandwidth f_B but also the bad signal-to-noise ratio (SNR) in STM preamplifiers.[4,13–16]

The bandwidth is limited by several factors simultaneously. First, $f_B \leq (2\pi R_F C_F)^{-1}$, where R_F is the feedback resistance and $C_F = (C_{AF} + C_{SF})$; in the latter, C_{AF} is from an artificially added feedback capacitor and C_{SF} is the unavoidable stray capacitance in the feedback loop wiring.[17] Specific methods to increase f_B include connecting many small resistance feedback resistors in series and multistage amplifying.[8] Second, f_B is also limited by $f_B \leq$ GBP/G, where GBP is the gain bandwidth product of the operational amplifier (OPA) and G is the noise gain of the amplifying circuit. This formula indicates that an OPA with higher GBP is required in the HS-STM preamplifier. Third, the STM preamplifier is a trans-impedance amplifier (TIA), while the preamplifier of the alternating current (AC)-STM belongs to the voltage amplifier.[18] Then, the bandwidth theory of TIA, which requires $f_B \leq (GBP/2\pi R_F C_S)^{1/2}$, has to be taken into account, where $C_S = C_{CM} + C_{DIFF} + C_j$ is the total source capacitance,[19,20] C_{CM} and C_{DIFF} separately are the common mode and differential mode input capacitance, and C_j (≈0.2 pF) is the tip–sample junction capacitance.[20] None of these bandwidth limitations can be ignored.

The authors have decreased the R_F from ∼ GΩ to 10 MΩ without the help of C_{AF}, and excellent STM images have been obtained,[11,21] but the bandwidth was only a little more than 10 kHz. The authors have also tried a 10 kΩ order R_F, which is frequently used in point contact mode STM/SPSTMs with several G_0 conductance[22–24] or μA tunneling current[22,25,26] (∼12.9 kΩ tunneling resistance[24]), to further increase the bandwidth. However, self-sustained oscillation (SSO) happens when the OPA model is OPA627 and there is no C_{AF}. Even more unfortunately, no phase compensation method is known to delete the SSO without a bandwidth cost, no matter internal compensation or external compensation.[27] The method of internal compensation by emitter degeneration, which is achieved by connecting a resistor in the emitter of the differential input stage of an OPA, will decrease the open-loop gain A_{OL} that indicates the superiority of the OPA. Internal dominant pole compensation, which is achieved by setting a capacitor in the intermediate stage, will decrease the GBP. External compensation by one-capacitor or two-capacitor is only suitable for voltage amplifiers. Limited by the above restrictions, the final bandwidth of the first stage (or the total) STM preamplifier is no more than 1 MHz. The highest frame frequency achieved is no more than 246 Hz,[9] and the highest line frequency is no more than 26 kHz[11] with poor atomic resolution.[11,28]

In this paper, the unique electronics property of the STM preamplifiers is analyzed. It varies at the different stages of the STM measurement. Then, the idea of paralleling a resistor with the tunneling junction (PRTJ) to delete the SSO is presented. This method results in the noise gain of the STM preamplifier increasing from unity to dozens. Counterintuitively, this increase is a good thing since it means that a high-rate, decompensated OPA with better antinoise ability can be used in the STM preamplifier. Finally, with the help of PRTJ and the decompensated OPA, up to 100 MHz ultrahigh bandwidth is achieved in the STM preamplifier, which is better than existing methods.[8,15,17] High-clarity, atomic-resolution quantum point contact microscopy (QPCM) imaging is achieved with record-breaking line frequency and frame frequency. QPCM is excellent in chemical sensitivity[22] and can be used to hear the audio frequency atom manipulation "sound" and investigate the origin of this "sound" better.[23]

II. PRINCIPLES AND DESIGN

A. Electronic properties of the STM preamplifier

The tip apex of the probe is far away from the sample initially in each STM measurement. Then, the coarse approach (CA) process is required, which makes the tip–sample distance smaller and smaller until the tunneling current is measurable. During this stage, the equivalent resistance $r_{jCA}(t)$ of the tunneling junction is close to ∞, and almost no tunneling current can be detected at this CA stage. This is a typical unstable state in electronics in which the noise gain $G = (1 + R_F/\infty) \sim 1$; this is called the *unity-gain* state. Unfortunately, the CA stage has seemed inevitable in STM measurements up to now.

The process following the CA stage is the scanning tunneling (ST) stage. The equivalent resistance $r_{jST}(t)$ of the tunneling junction is usually much less than the resistance R_F. Then, the noise gain of the STM preamplifier usually is dozens, which results in the STM preamplifier being in a normal TIA state.

B. Unity gain stable amplifiers

The unstable unity-gain state requires a special unity-gain-stable (UGS) OPA under current STM preamplifier technology. UGS-OPA is a performance-compromised version of an OPA, designed for barely sufficient stability by complete compensation by the decompensated OPA. The UGS-OPA and decompensated OPA mostly appear in pairs.[27,30,31] The decompensated OPA has almost all the advantages over the UGS-OPA except that the hash required a minimum noise gain G_{min}. For example, higher GBP, higher slew rate (SR), and less settling time (ST) indicate the speed superiority of the decompensated OPA. The higher open-loop gain A_{OL}, less total harmonic distortion and noise (THD + N), higher common-mode rejection ratios (CMRR), and the higher maximum output voltage u_{omax} indicate the other superiority of the decompensated OPA. As an example, OPA627 (a UGS-OPA) and OPA637 (a decompensated OPA) are compared, as shown in Table I. The bottom line of the first line of the table is the test conditions. OPA637 is dozens of times better than OPA627 in multiple indicators. It is a huge loss that decompensated OPAs could not be used in STM preamplifiers before now, especially in HS-STMs.

C. STM preamplifier designs

SSO happens when both the amplitude condition and the phase condition are satisfied in the STM preamplifier at the same time,

TABLE I. Advantages of decompensated OPA over UGS-OPA, taking OPA627 and OPA627 as examples.

	GBP (MHz)	SR (V/μs)	ST (μs)	A_{OL} (dB)	THD + N (ppm)	CMRR (dB)	u_{omax} (V)	
Type of OPA	25 °C	25 °C	G = −10	20 kHz	20 kHz	20 kHz	7 MHz	G_{min}
OPA627BP (UGS type)	16	16	1.2	23	50	100	3	1
OPA637BP (Decompensated)	80	99	0.6	34	10	120	6	5

regardless of whether the OPA is UGS.[27,32] In this situation, the minimum noise gain requirement of the picky decompensated OPA inversely indicates that increasing the noise gain can make the STM preamplifier more stable.[30]

A resistor is connected in parallel with the tunneling junction to increase the noise gain of the STM preamplifier. The bias voltage U_B can be set in multiple ways, one of which is shown in Fig. 1. To better characterize the tunneling junction to be measured, the resistor mentioned above has to have constant resistance, noted as R_0.

The noise gain will increase from 1 to $(1 + R_F/R_0)$ at the CA stage because of the parallel resistor configuration, which we denote by $r_j(t)//R_0$. This means that UGS-OPAs are no longer required. Instead, decompensated OPAs can be used not only to increase the f_B but also to augment the antinoise ability in the STM preamplifier, as shown in Fig. 1.

The output $u_O(t)$ of this $r_j(t)//R_0$ STM preamplifier can be divided into two parts $u_{OSTM}(t)$ and U_{OR0} in theory by the superposition theorem: $u_O(t) = u_{OSTM}(t) + U_{OR0}$. Constant $U_{OR0} = U_B \times (1 + R_F/R_0)$ is caused by the constant current I_{R0}, which flows through the constant resistor R_0, as shown in Fig. 1. This U_{OR0} value is independent of what sample is scanned, so it can be deleted to increase the contrast of the sample signal. The $u_{OSTM}(t)$, which is caused by the tunneling current $i_j(t)$ that flows through the tunneling junction $r_j(t)$, is the same as the output of a traditional STM preamplifier, as shown in Fig. 1. The bad effect of the thermal noise current in the constant resistance R_0 will be analyzed in Sec. II D.

D. *SNR* analysis of the $r_j(t)//R_0$ STM preamplifier

The thermal noise current caused by the constant resistance R_0 can be calculated by $i_{nR0} = (4kTf_B/R_0)^{1/2} = 1.62 \times 10^{-4}/(R_0R_F)^{1/2}$, where $k = 1.38 \times 10^{-23}$ J/K, $T \approx 300$ K, and $f_{Bmax} = 1/2\pi R_F C_{sF} \approx 1.6 \times 10^{12}/R_F$ for$C_{sF} \approx 0.1$ pF[21]. If $R_F/R_0 = N$, then $i_{nR0max} = 1.62 \times 10^{-4} \times N^{1/2}/R_F$, where N is a constant. The signal of the STM output mentioned above can be ideally expressed as simple harmonic $u_{OSTM}(t) = U_A \sin 2\pi ft + U_C$, while the frequency f, amplitude U_A, and offset U_C may vary when the STM tip apex is scanning from one atom to another atom.

The only part that reflects the resolution of the STM is the AC component $U_A \sin 2\pi ft$. Then, the effective value of the tunneling current $i_j(t)$ can be expressed as $i_j(t) = U_A/\sqrt{2}R_F$. The negative effect of R_0 on the *SNR* can be calculated as $SNR_{R0min} = (U_A/\sqrt{2}R_F)/i_{nR0max} = 4.4 \times 10^3 \times N^{-1/2} U_A$. Because N is usually about 10, the fact that 100 mV U_A is moderate in most STM measurements will make the *SNR* rise to about 100. When operated under LHe temperature, the *SNR* will increase tenfolds. The higher CMRR, higher A_{OL}, and lower THD + N of the decompensated OPA compared to the traditional UGS-OPA will further ensure the high *SNR*.

III. RESULTS AND DISCUSSION

A. Higher stability STM preamplifier

The stability of our $r_j(t)//R_0$ STM preamplifier was verified first with a traditional UGS-OPA. The results are measured with a Tektronix TDS 3014C oscilloscope. SSO happens at about 90 kHz when OPA627 and a 1 MΩ feedback resistance R_F is used. The wave resembles a square wave and is caused by the over saturated output of a sine wave, which is chopped, as shown in Fig. 2. The amplitude is so high that the scale rises to 3 V, as shown on the left side. The peak-to-peak value is still as high as about 13 V after being chopped, which means that no signal can be amplified and output in the conventional STM preamplifier circuit.

When a 100 kΩ R_0 is introduced, SSO is eliminated. Then, a voltage amplifier is formed at the CA stage with no measurable tunneling current. The output is so small that the scale is only 0.1 V, as shown in Fig. 2 on the right-hand side. The straight horizontal line output is mainly caused by the offset of the $r_j(t)//R_0$ STM preamplifier. No special shock absorption and electromagnetic shielding are needed, except that the STM preamplifier circuit box is made of cast aluminum. The alternating current component has strength no more than 10 mV, which is the noise of the system.

The phase compensation achieved by the single resistor R_0 is different from the existing compensation methods, both internally and externally.[27] It can also be used in other TIAs to increase their stability.

B. Radio frequency bandwidth STM preamplifier

Decompensated OPAs, such as OPA637 or OPA657, can be introduced into the STM preamplifier to achieve higher bandwidth and higher *SNR* for the first time, benefiting from the highly stable $r_j(t)//R_0$ design.[21] The higher stability enables the R_F value to

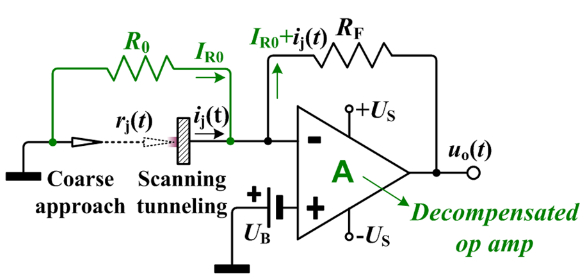

FIG. 1. Schematic diagram of the $r_j(t)//R_0$ STM preamplifier. $r_j(t)$ represents the equivalent resistance of the tunneling junction. U_B is the bias voltage. The $\pm U_S$ are the positive and negative power supplies. A decompensated operational amplifier is used in the STM preamplifier. The gradually changing shadow between the tip and sample illustrates the trend of the tunneling probability.

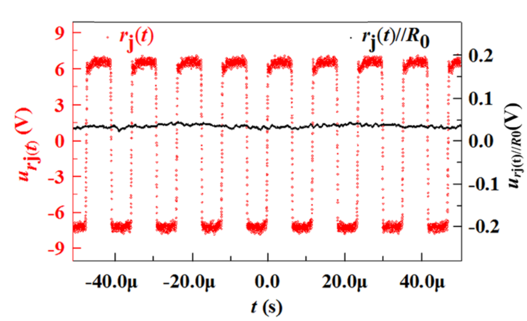

FIG. 2. Comparison of stability between the traditional and $r_j(t)//R_0$ STM preamplifier. Both waves are characterized using an oscilloscope.

decrease from 1 MΩ to 10 kΩ, which further increases the f_B. The resistor R_0 in both circuits has resistance 1 kΩ.

Power spectral density measurements are used to characterize the bandwidth, as shown in Figs. 3(a) and 3(b). The bandwidths are about 8.9 MHz and 166 MHz. The three peaks in Fig. 3(b) may be caused by the potential instability in the corresponding frequency. The ultrahigh 166 MHz f_B fits well with both the theory of $f_B = (2\pi R_F C_{sF})^{-1}$ = 159 MHz and the theory of $f_B \leq \mathrm{GBP/G} \approx 145$ MHz, where the GBP of OPA657 is 1.6 GHz.

Both bandwidths are also analyzed by the Bode diagram of the $r_j(t)//R_0$ STM preamplifier under the single-pole OPA model and the $A_{OL} \gg 1$ assumption.[19] When R_0 is introduced, the total input impedance changes from X_{CS} to $X_{CS}//R_0$. However, the expression of the transfer function of the STM preamplifier[19] is still intact: $u/i = \omega_0^2 R_F/(s^2 + s\omega_0/Q + \omega_0^2)$ with intact $\omega_0^2 = 2\pi\mathrm{GBP}/[R_F(C_F + C_S)]$, where s = iω. Only the expression of the quality factor Q changed slightly, by $R_F//R_0$, into

$$Q \approx [2\pi \times \mathrm{GBP} \times R_F \times (C_F + C_S)]^{1/2}/(1 + R_F/R_0 + 2\pi \times \mathrm{GBP} \times R_F \times C_F).$$

When OPA637 is used, Q and ω_0 are about 0.76 rad/s and 57.4 rad/s, respectively; when OPA657 is used, Q and ω_0 are about 1.12 rad/s and 428 rad/s, respectively. Substituting each Q and ω_0 into the transfer function, we get $u/i_{\mathrm{OPA637}} = 3.28 \times 10^{19}/(s^2 + 7.52 \times 10^7\ s + 3.28 \times 10^{15})$ and $u/i_{\mathrm{OPA657}} = 1.8 \times 10^{19}/(s^2 + 2.3 \times 10^8\ s + 1.8 \times 10^{17})$. The magnitude parts of each transfer function indicate that the bandwidths are about 9.3 MHz and 100 MHz, as shown in Figs. 3(c) and 3(d). The bandwidth of 9.3 MHz is in good agreement with the data in Fig. 3(a). We note that 100 MHz is less than 166 MHz; the lower value may result from the crude assumption of the single-pole OPA model, as shown by the single pole in Fig. 3(d).

The frequency 166 MHz f_B is so high that it becomes a challenge for other parts of the HS-STM system, such as the scanner and data acquisition (DAQ) card.[9] The DAQ card in our HS-STM system is a PXI-6124 whose sampling rate is 4 MS/s. The resonant frequency of the scanner is about 100 kHz.

C. Quantum point contact mode HS-STM

The performance of the $r_j(t)//R_0$ STM preamplifier was also confirmed by our home-built HS-STM[11] We used parameters R_F = 10 kΩ, R_0 = 1 kΩ, and C_{AF} = 0 pF, and an OPA637 was used, resulting in a bandwidth of about 9 MHz, as mentioned above and as shown in Figs. 3(a) and 3(c). High-clarity atomic resolution images are obtained, which have almost the same quality as those obtained using the conventional STM preamplifier,[33] as shown in Figs. 4(a)–4(e). The frequency 9 MHz had broken the bandwidth record for an atomic resolution HS-STM.

The images, which were raw data of a highly oriented pyrolytic graphite (HOPG) sample, were obtained in air under room temperature with a mechanically cut Pt/Ir tip. The bias voltage was −220 mV. The different brightness areas in the image may be caused by the obliqueness of the sample. One of the most noteworthy reflections of the performance of the STM system was the peak–peak voltage $u_{pp} = 2U_A$. The compromise magnitude in the line cut profile is $u_{pp} \cong 140$ mV, as shown in Fig. 4(b). The 70 mV U_A indicates that the SNR_{R0min} is $4.4 \times 10^3 \times N^{-1/2} U_A = 97$, which means that the noise caused by R_0 is not worth worrying about at all.

All the images in Fig. 4 were measured under a record-breaking frame rate of 250 frame/s[4,9] and a record-breaking line rate of 50 k

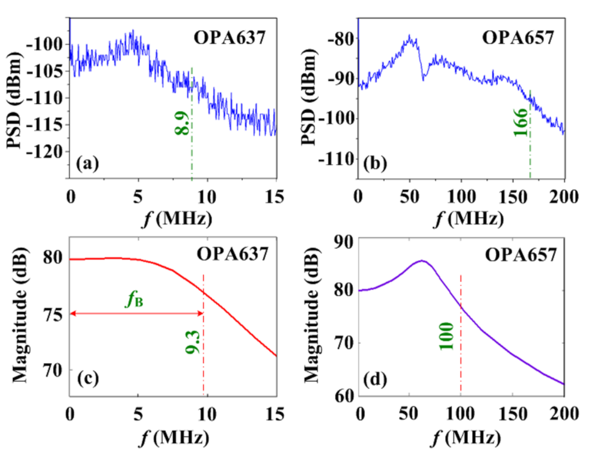

FIG. 3. Power spectral density measurements and Bode diagrams of $r_j(t)//R_0$ STM preamplifiers. (a) and (b) are the PSD measurements. (c) and (d) are the Bode diagrams. (a) and (c) are the output measured and calculated for the STM preamplifier based on OPA637. (b) and (d) are the output measured and calculated for the STM preamplifier based on OPA657.

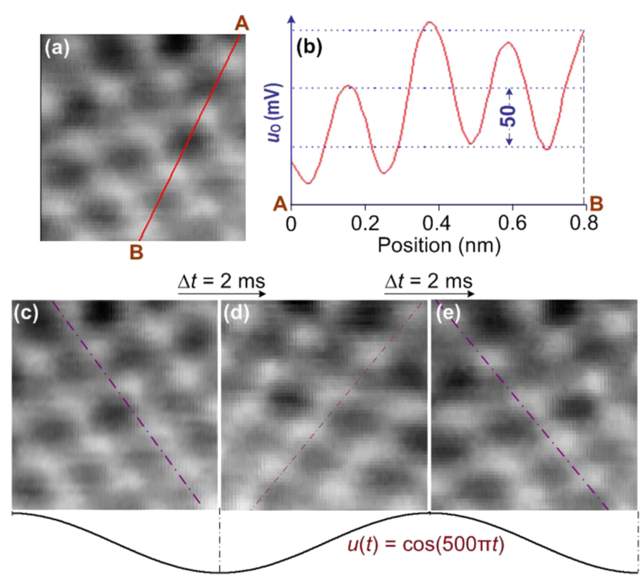

FIG. 4. The $r_j(t)//R_0$ HS-STM image (raw data) based on the decompensated OPA. The sample is HOPG. (a) One frame HS-STM atomic resolution image (under conditions: 50 kHz fast scanning frequency, 250 Hz slow scanning frequency, 7.5 Å × 7.2 Å). (b) Profile along the line AB in (a). About 150 mV u_{pp} is scaled to indicate the SNR of the STM system. U_B = −220 mV. The lateral distance along the horizontal-axis is 7.9 Å. (d) is the opposite frame in the same period with (c). The time difference Δt between (c) and (d) is 2 ms, which is half of the period. (e) is the image in the next half period of (d). The sine wave and the dotted lines in the atomic resolution images show the corresponding direction of scanning in the slow axis.

line/s;[11,34] both benefited from the unrestrained high bandwidth of the $r_j(t)//R_0$ STM preamplifier.

A continuous scanning on the HOPG surface was also performed with a record-breaking slow axis scanning frequency of 250 Hz, as shown in Figs. 4(c)–4(e). There is little difference between each image. The frame frequency is twice as the scanning frequency to 500 Hz when counting the frames that are going back and forth, as shown in Figs. 4(c) and 4(d).

The 70 mV U_A indicates that the effective value of the tunneling current signal is $U_A/\sqrt{2}R_F = 5\ \mu A$. This signal value means that the equivalent conductance of the tunneling junction is about $0.3G_0$, which indicates that this STM is operating under the quantum point contact state. QPCM can be applied to many fields of surface science. For example, the tribological characteristic, which is related to speed,[35,36] has been expressed in terms of current.[37,38] As for the open problem of application with a weak tunneling current, multistage amplification can be employed. This improvement is our next goal.

IV. CONCLUSION

The higher stability of the $r_j(t)//R_0$ STM preamplifier was analyzed and testified, showing that it can increase the bandwidth. This research shows that a superior-performance, decompensated OPA can be used to further increase the bandwidth and the SNR of the STM preamplifier. The recording-break line rate and frame rate atomic resolution HS-STM images indicate that more interesting and important effects will be revealed. The $r_j(t)//R_0$ method and decompensated OPA can also be generalized to almost all other types of STM preamplifiers to increase the SNR.

ACKNOWLEDGMENTS

This work was supported by the National Natural Science Foundation of China (Grant Nos. 11304082, U1932216, and 51627901), the National Key R&D Program of China (Grant Nos. 2017YFA0402903 and 2016YFA0401003), the Scientific Research Equipment Developing Project of the Chinese Academy of Sciences (Grant No. YZ201628), the Maintenance and Renovation Project for CAS Major Scientific and Technological Infrastructure (Grant No. DSS-WXGZ-2019–0011), and the Science and Technology Department of Henan Province (Grant Nos. 182102210367 and 182102210370).

DATA AVAILABILITY

The data that support the findings of this study are openly available upon reasonable request.

REFERENCES

[1] L. Gao *et al.*, "Constructing an array of anchored single-molecule rotors on gold surfaces," Phys. Rev. Lett. **101**, 197209 (2008).

[2] R. Ma *et al.*, "Atomic imaging of the edge structure and growth of a two-dimensional hexagonal ice," Nature **577**, 60–63 (2020).

[3] F. E. Kalff, M. P. Rebergen, E. Fahrenfort, J. Girovsky, R. Toskovic, J. L. Lado, J. Fernández-Rossier, and A. F. Otte, "A kilobyte rewritable atomic memory," Nat. Nanotechnol. **11**, 5 (2016).

[4] L. L. Patera, F. Bianchini, C. Africh, C. Dri, G. Soldano, M. M. Mariscal, M. Peressi, and G. Comelli, "Real-time imaging of adatom-promoted graphene growth on nickel," Science **359**, 1243 (2018).

[5] J. C. Gehrig *et al.*, "Surface single-molecule dynamics controlled by entropy at low temperatures," Nat. Commun. **8**, 14404 (2017).

[6] C. Martin, J. W. W. Fischer, F. E. Robles, and W. S. Warren, "Invited review article: Pump-probe microscopy," Rev. Sci. Instrum. **87**, 031101 (2016).

[7] J. Friedlein, J. Harm, P. Lindner, L. Bargsten, M. Bazarnik, S. Krause, and R. Wiesendanger, "A radio-frequency spin-polarized scanning tunneling microscope," Rev. Sci. Instrum. **90**, 123705 (2019).

[8] C. Xu, Y. Que, Y. Zhuang, K. Wang, and X. Xiao, "Construction of a gigahertz-bandwidth radio-frequency scanning tunneling microscope based on a commercial low-temperature system," Rev. Sci. Instrum. **90**, 103706 (2019).

[9] F. Esch *et al.*, "The FAST module: An add-on unit for driving commercial scanning probe microscopes at video rate and beyond," Rev. Sci. Instrum. **82**, 053702 (2011).

[10] C. Dri *et al.*, "The new FAST module: A portable and transparent add-on module for time-resolved investigations with commercial scanning probe microscopes," Ultramicroscopy **205**, 49–56 (2019).

[11] Q. Li and Q. Lu, "Atomic resolution ultrafast scanning tunneling microscope with scan rate breaking the resonant frequency of a quartz tuning fork resonator," Rev. Sci. Instrum. **82**, 053705 (2011).

[12] K. M. Bastiaans, T. Benschop, D. Chatzopoulos, D. Cho, Q. Dong, Y. Jin, and M. P. Allan, "Amplifier for scanning tunneling microscopy at MHz frequencies," Rev. Sci. Instrum. **89**, 093709 (2018).

[13] G. Schitter and M. J. Rost, "Scanning probe microscopy at video-rate," Mater. Today **11**, 40–48 (2008).

[14] F. Massee, Q. Dong, A. Cavanna, Y. Jin, and M. Aprili, "Atomic scale shot-noise using cryogenic MHz circuitry," Rev. Sci. Instrum. **89**, 093708 (2018).

[15] J. B. Martin Štubian, S. Martin, U. Diebold, and M. Schmid, "Fast low-noise transimpedance amplifier for scanning tunneling microscopy and beyond," Rev. Sci. Instrum. **91**, 074701 (2020).

[16] J. P. Petersen and S. A. Kandel, "Circuit design considerations for current preamplifiers for scanning tunneling microscopy," J. Vac. Sci. Technol., B **35**, 033201 (2017).

[17] U. Kemiktarak, T. Ndukum, K. C. Schwab, and K. L. Ekinci, "Radio-frequency scanning tunnelling microscopy," Nature **450**, 85 (2007).

[18] L. L. Patera, F. Queck, P. Scheuerer, and J. Repp, "Mapping orbital changes upon electron transfer with tunnelling microscopy on insulators," Nature **566**, 245–248 (2019).

[19] X. Ramus, *Transimpedance Considerations for High-Speed Amplifiers* (Texas Instruments Incorporated, 2009), Vol. SOBA122.

[20] J. M. de Voogd *et al.*, "Fast and reliable pre-approach for scanning probe microscopes based on tip-sample capacitance," Ultramicroscopy **181**, 61–69 (2017).

[21] Q. Li, Q. Wang, Y. Hou, and Q. Lu, "18/20 T high magnetic field scanning tunneling microscope with fully low voltage operability, high current resolution, and large scale searching ability," Rev. Sci. Instrum. **83**, 043706 (2012).

[22] Y.-h. Zhang, P. Wahl, and K. Kern, "Quantum point contact microscopy," Nano Lett. **11**, 3838–3843 (2011).

[23] J. Bork *et al.*, "A tunable two-impurity Kondo system in an atomic point contact," Nat. Phys. **7**, 901–906 (2011).

[24] S. Ouazi, A. Kubetzka, K. von Bergmann, and R. Wiesendanger, "Enhanced atomic-scale spin contrast due to spin friction," Phys. Rev. Lett. **112**, 076102 (2014).

[25] M. Enachescu, D. Schleef, D. F. Ogletree, and M. Salmeron, "Integration of point-contact microscopy and atomic-force microscopy: Application to characterization of graphite/Pt(111)," Phys. Rev. B **60**, 16913–16919 (1999).

[26] N. Agraït, J. G. Rodrigo, and S. Vieira, "On the transition from tunneling regime to point-contact: Graphite," Ultramicroscopy **42-44**, 177–183 (1992).

[27] J. Karki, Using a Decompensated Operational Amplifier for Improved Performance, Texas Instruments SLYT015, 2001.

[28] F. Besenbacher, E. Lægsgaard, and I. Stensgaard, "Fast-scanning STM studies," Mater. Today **8**, 26–30 (2005).

[29]J. A. Stroscio and R. J. Celotta, "Controlling the dynamics of a single atom in lateral atom manipulation," Science **306**, 242 (2004).
[30]Precision High-Speed Difet Operational Amplifiers of OPA627 and OPA637, www.ti.com, 1998.
[31]OPA657 1.6-GHz, Low-Noise, FET-Input Operational Amplifier, www.ti.com, 2015.
[32]A. Bhat, *Stabilize Your Transimpedance Amplifier* (Maxim Integrated, 2012).
[33]J. Wang, W. Ge, Y. Hou, and Q. Lu, "Scanning tunneling microscopy evidences for surface electron scattering by underlying atoms," Carbon **84**, 74–81 (2015).
[34]A. van Houselt and H. J. W. Zandvliet, "Colloquium: Time-resolved scanning tunneling microscopy," Rev. Mod. Phys. **82**, 1593–1605 (2010).
[35]D. Gangloff, A. Bylinskii, I. Counts, W. Jhe, and V. Vuletić, "Velocity tuning of friction with two trapped atoms," Nat. Phys. **11**, 915–919 (2015).
[36]X. Z. Liu *et al.*, "Dynamics of atomic stick-slip friction examined with atomic force microscopy and atomistic simulations at overlapping speeds," Phys. Rev. Lett. **114**, 146102 (2015).
[37]E. Gnecco, M. Kisiel, U. Gysin, L. Marot, S. Rast, and E. Meyer, "Suppression of electronic friction on Nb films in the superconducting state," Nat. Mater. **10**, 119 (2011).
[38]J. Y. Park, D. F. Ogletree, P. A. Thiel, and M. Salmeron, "Electronic control of friction in silicon pn junctions," Science **313**, 186 (2006).